Extended-State-Observer-Based Double-Loop Integral Sliding-Mode Control of Electronic Throttle Valve

Yongfu Li, Bin Yang, Taixiong Zheng, Yinguo Li, Mingyue Cui, and Srinivas Peeta

***Abstract*—An extended-state-observer-based double-loop integral sliding-mode controller for electronic throttle (ET) is proposed by factoring the gear backlash torque and external disturbance to circumvent the parametric uncertainties and nonlinearities. The extended state observer is designed based on a nonlinear model of ET to estimate the change of throttle opening angle and total disturbance. A double-loop integral sliding-mode controller consisting of an inner loop and an outer loop is presented based on the opening angle and opening angle change errors of ET through Lyapunov stability theory. Numerical experiments are conducted using simulation. The results show that the accuracy and the response time of the proposed controller are better than those of the back-stepping and sliding mode control.**

***Index Terms*—Double-loop integral sliding-mode control (DLISMC), extended state observer (ESO), electronic throttle (ET) control.**

I. Introduction

UNDER intelligent transportation systems (ITS), vehicle-to-vehicle (V2V) communications can play an important role in the coordination between individual vehicles as well as between the vehicles and the roadside infrastructure. For example, to avoid collisions in vehicular traffic flow, a wide variety of information is desirable from preceding vehicles and roadside equipment by leveraging V2V communications [1]–[3]. In this context, the V2V-based communication of information on the opening angle of the electronic throttle (ET) of the preceding vehicles in a lane enables a following vehicle in that platoon to react autonomously to avoid a collision by adjusting adaptively its ET. This is because the electronic throttle control (ETC) is the core of the vehicle control and past studies [4]–[6] illustrate that the vehicle speed is related to the opening angle of the ET.

This study is motivated by the need for a more accurate and responsive controller so that platoon stability can be improved under a stimulus through V2V information communication related to the ET opening angle. Past studies [7], [8] on ET show that the accuracy of the controller is important to improve the stability and robustness of the ET system. Thereby, the stability of the vehicle speed can be enhanced through smooth changes. However, multiple nonlinearities and uncertainties including stick-slip friction, gear backlash, and nonlinear spring [9], [10] adversely affect the accuracy of the ETC. In terms of the response time of the controller, studies [11]–[13] on vehicle platoon control suggest that it is desirable for all vehicles in the platoon to move with a safe space headway and a safe speed from a stability perspective. However, under a stimulus such as an accident just in front of a platoon, the lead vehicle in the platoon must brake immediately as an emergency response maneuver to avoid the accident. The following vehicles in the platoon will then respond accordingly. Hence, a quick response time is desirable for the ET controller to enhance platoon stability. This study focuses on developing a more accurate and responsive ET controller.

Several control strategies have been proposed to improve the performance in terms of the accuracy and responsiveness of the ETC, including linear control, nonlinear control, optimal control and intelligent control. From the linear control perspective, Deur *et al.* [10] designed an optimized proportional-integral-derivative (PID) controller that compensates the effects of friction and limp-home using a feedback compensator. However, the friction compensator is prone to high-frequency oscillations under steady-state conditions, which are not transferred to the output signal practically. Yuan *et al.* [14] proposed a neural network based self-learning PID controller. However, the back propagation (BP) algorithm used in the neural network can deteriorate the performance of the controller [15]–[17]. Sheng *et al.* [18] proposed a fractional order fuzzy-PID controller for ET and used the fruit fly optimization algorithm to search for the optimal values of the controller parameters. However, the gear backlash torque, which plays an important

Manuscript received June 30, 2014; revised September 19, 2014, October 31, 2014, and February 8, 2015; accepted February 27, 2015. Date of publication March 24, 2015; date of current version September 25, 2015. This work was supported in part by the National Natural Science Foundation of China under Grant 61304197, by the Scientific and Technological Talents of Chongqing under Grant cstc2014kjrc-qnrc30002, by the Key Project of Application and Development of Chongqing under Grant cstc2014yykfB40001, by the Natural Science Funds of Chongqing under Grant cstc2014jcyjA60003, and by the U.S. Department of Transportation (U.S. DOT) through the NEXTRANS Center (the U.S. DOT Region 5 University Transportation Center). The Associate Editor for this paper was B. De Schutter.

Y. Li is with the College of Automation and Center for Automotive Electronics and Embedded System, and also with the Electronic Information and Networking Research Institute, Chongqing University of Posts and Telecommunications (CQUPT), Chongqing 400065, China (e-mail: liyongfu@cqupt.edu.cn).

B. Yang, T. Zheng, and Y. Li are with the College of Automation and Center for Automotive Electronics and Embedded System, Chongqing University of Posts and Telecommunications, Chongqing 400065, China (e-mail: zhengtx@cqupt.edu.cn; liyg@cqupt.edu.cn).

M. Cui is with the College of Physics and Electronic Engineering, Nanyang Normal University, Nanyang 473061, China (e-mail: cuiminyue@sina.com).

S. Peeta is with the School of Civil Engineering and the NEXTRANS Center, Purdue University, West Lafayette, IN 47907 USA (e-mail: peeta@purdue.edu).

Color versions of one or more of the figures in this paper are available online at http://ieeexplore.ieee.org.

Digital Object Identifier 10.1109/TITS.2015.2410282

role in the controller design, is ignored in this control strategy. Yadav *et al.* [19] incorporated the ETC into an uncertain hybrid electric vehicle (HEV) speed control, where a self-tuning fuzzy PID controller and model reference adaptive systems with sliding mode adaptation mechanisms are developed to achieve robust performance of the ET-controlled HEV. However, the use of the sign function in the sliding mode control (SMC) leads to high-frequency chattering which affects control performance due to the discontinuous control when the system states approach the sliding surface.

From the nonlinear control perspective, Barić *et al.* [20] proposed a high-performance ETC strategy based on an extended SMC with a neural network which compensates for uncertainties including friction and limp-home. However, it requires high computational power due to the quasi-continuous-time implementation (i. e., a very small sampling time). Moreover, the control scheme does not explicitly take into account the constraints on process variables. To account for the process variable constraints, Pan *et al.* [21] designed a sliding mode observer (SMO) based variable structure control (VSC) to estimate the opening angle change of the ET valve. However, they only consider the Coulomb friction in the friction torque, and ignore the stick-slip friction, which has a significant effect on friction torque. In addition, the phenomenon of chattering occurs due to the nature of VSC with high gain. Chen *et al.* [22] investigated the ETC using the back-stepping method, and proposed guidelines for selecting the controller parameters based on input-to-state-stable (ISS) theory. However, the designed controller does not consider the unmodeled dynamics and unknown disturbances, which was only considered in the ISS analysis instead of the controller design. Therefore, the disturbance in practice would lead to the deterioration of robustness.

On the basis of optimal control, Vašak *et al.* [23] presented the constrained finite-time optimal control method, which addresses the gearbox friction and limp-home nonlinearity by solving a constrained optimal control problem formulated for the discrete-time piecewise affine model of the throttle. The drawback of this approach is that it relies excessively on the model. Hence, if the model accuracy declines, it would lead to significant performance deterioration. To address this issue, Vašak *et al.* [24] proposed a model predictive control based time-optimal control strategy to improve the controller performance. Kim *et al.* [9] proposed a dynamic programming based optimal controller for the ET valve. It uses dynamic programming to obtain the optimal gear shift and throttle opening angle and develop throttle/gear maps that satisfy the driver's power demand. However, it does not provide enough power since the maps lack a self-learning capability.

Recently, intelligent control has been widely used in engine control through controller design, parameter identification and fault diagnosis. Yuan *et al.* [25], [26] proposed a neural network based ETC, which can circumvent the influence of both plant parameter variations and operation state changes on the ETC performance. However, the BP algorithm leads to slow training and also results in a local minimum. Wang *et al.* [27] suggested an intelligent fuzzy controller with feedforward closed-loop configuration to deal with the nonlinear hysteretic behavior of ET. They also proposed a new closed-loop back-propagation tuning for the fuzzy output membership function to obtain better tracking performance. However, the designed fuzzy rule about the feedforward controller is too simple to illustrate the condition of nonlinear hysteresis.

The literature review heretofore illustrates that the ETC accuracy and responsiveness challenges arise from the nonlinearities and uncertainties such as the stick-slip friction, gear backlash and nonlinear spring. Hence, motivated by the V2V context, this study seeks to reduce the influence of parametric uncertainties and the nonlinearities. Specifically, an ESO is designed to estimate the throttle opening angle change and total disturbance with the consideration of its active disturbance rejection. The study proposes the double loop integral sliding mode control (DLISMC) that includes an inner-loop and an outer-loop, based on the opening angle and corresponding change errors of the ET valve according to the Lyapunov stability theory.

The primary study objective is to present a novel nonlinear controller for the ET based on SMC and ESO. The proposed controller is deployable as it meets the requirements in the engineering practice context [10]. The study contributions are as follows. First, in the ET controller design, many previous studies [10], [14], [18]–[22], [25]–[27] treat only the throttle opening angle error as feedback, and do not consider the throttle opening angle change error. To the best of our knowledge, this study is the first to consider both the throttle opening angle error and the throttle opening angle change error as feedback. Accordingly, in our double closed loop controller, the inner loop controller is based on throttle opening angle change error and the outer loop controller is based on the throttle opening angle error. Thereby, the controller can track the throttle opening angle and opening angle change simultaneously to enhance the accuracy of the proposed controller. Second, the integral term, which can effectively eliminate the static error of the system, is incorporated into the sliding mode surface design, resulting in improved ET system stability. Third, the gear backlash torque and external disturbance are taken into consideration to reduce the effects of parametric uncertainties and nonlinearities.

The rest of this paper is organized as follows. In Section II, the mathematical model of the ET valve system including the friction and nonlinear spring model is presented. The DLISMC controller with the ESO is designed in Section III. Section IV performs numerical simulation experiments and compares the performance of the proposed controller with those of the back-stepping and SMC controllers. The final section provides some concluding comments.

II. Model

An ET system consists of a dc drive (powered by the chopper), a gearbox, a valve plate, a dual return spring, and a position sensor [14], [23], [24]. Fig. 1 shows the functional scheme of the ET.

According to Kirchhoff's law, below is the description of the motor winding circuit [22], [24]

$$L_a \frac{\mathrm{d}i_a}{\mathrm{d}t} + R_a i_a = k_{ch} u - k_v \dot{\theta}_m \tag{1}$$

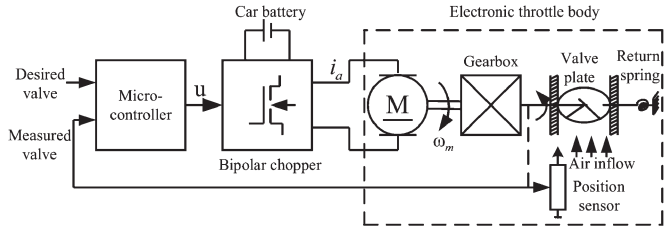

Fig. 1. Schematic of electronic throttle.

where L_a and R_a are the armature inductance and the overall resistance of the armature circuit, respectively. And i_a, u represent the dc motor armature current and the input control voltage, respectively. k_{ch} and k_v denote the chopper gain and the electromotive force constant, respectively, and $\dot{\theta}_m$ is the motor angular velocity.

In terms of the torque balance principle, the kinematic differential equation of ET valve is [22], [24]

$$Jk_l^2\ddot{\theta} = k_l k_t i_a - m_s - m_f - m_g \tag{2}$$

where θ is the position (opening angle) of ET, J is the overall moment of inertia referred to the motor side, k_t is the motor torque constant, m_s is the throttle return spring torque, m_g is the unknown gear backlash torque, and $k_l = \theta_m/\theta$ is gear ratio. m_f is the frictional torque caused by Coulomb and sliding friction as in [22]

$$m_f = k_{tf}\mathbf{sgn}(\dot{\theta}) + k_f\dot{\theta} \tag{3}$$

where k_{tf} is Coulomb friction coefficient and k_f is sliding friction coefficient.

The throttle return spring torque m_s is given by [22]

$$m_s = k_{sp}(\theta - \theta_0) + k_{pre}\mathbf{sgn}(\theta - \theta_0) \tag{4}$$

where k_{sp} is spring elastic coefficient, k_{pre} is the spring tightening torque coefficient, and θ_0 is the default opening angle of the throttle plate.

The system sampling time is chosen with respect to the dominant time constant of the linearized ET model and is set to $T = 5$ ms [10]. The armature current dynamics can be neglected since the time constant $T_a = L_a/R_a \le T$. Therefore, (1) can be simplified as

$$i_a = \frac{1}{R_a}\left(k_{ch}u - k_v\dot{\theta}_m\right). \tag{5}$$

Based on (2)–(5), the ET model is

$$\ddot{\theta} = \frac{1}{k_l^2 J}\left[\frac{k_l k_t k_{ch}}{R_a}u - \left(\frac{k_l^2 k_t k_v}{R_a} + k_f\right)\dot{\theta} - m_g - k_{sp}(\theta - \theta_0) - k_{pre}\mathbf{sgn}(\theta - \theta_0) - k_{tf}\mathbf{sgn}(\dot{\theta})\right]. \tag{6}$$

Then, let $x_1 = \theta$ and $x_2 = \dot{\theta}$. By considering the external disturbance $d(t)$, (6) can be rewritten as

$$\begin{cases} \dot{x}_1 = x_2 \\ \dot{x}_2 = a_{21}(x_1 - \theta_0) + a_{22}x_2 + bu + \kappa_2\mathbf{sgn}(x_2) \\ \qquad + \kappa_1\mathbf{sgn}(x_1 - \theta_0) + \kappa_3 m_g + d(t) \end{cases} \tag{7}$$

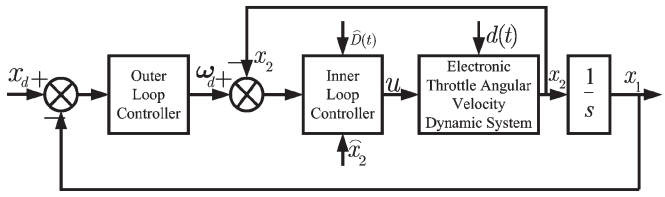

Fig. 2. ETC strategy.

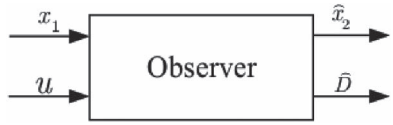

Fig. 3. Structure of observer.

where $a_{21} = -(k_{sp}/k_l^2 J)$, $a_{22} = -((k_l^2 k_t k_v + k_f R_a)/(k_l^2 J R_a))$, $b = (k_t k_{ch}/k_l J R_a)$, $\kappa_1 = -(k_{pre}/k_l^2 J)$, $\kappa_2 = -(k_{tf}/k_l^2 J)$, $\kappa_3 = -(1/k_l^2 J)$, $|d(t)| \le L$.

(7) can be rewritten as

$$\begin{cases} \dot{x}_1 = x_2 \\ \dot{x}_2 = a_{21}(x_1 - \theta_0) + a_{22}x_2 + bu + \kappa_2\mathbf{sgn}(x_2) \\ \qquad + \kappa_1\mathbf{sgn}(x_1 - \theta_0) + D(t) \end{cases} \tag{8}$$

where $D(t) = \kappa_3 m_g + d(t)$ is total uncertainty of ET, and $D \le \|M\|$.

III. Controller Design

Given the accuracy and responsiveness requirements, and the practical difficulty in measuring the opening angle change of ET and the total disturbance [21], [22], ESO is used to carry out the estimation [28]–[31]. Fig. 2 illustrates the control strategy of ET, where $\widehat{x}_2$ is the estimation of the ET opening angle change, which cannot be measured practically. $\widehat{D}(t)$ is the estimation of total disturbance $D(t)$ which is a critical factor but neglected in the high precision controller design.

A. Observer Design

1) Observer Design and Stability Analysis: ESO plays an important role in the active disturbance reduction controller, which can estimate the state of control system as well as the disturbance. The structure of ESO is shown in Fig. 3.

According to (8), the ESO is designed as a variant of [32]–[34] by additionally considering $\widehat{D}$

$$\begin{cases} \dot{\widehat{x}}_1 = \widehat{x}_2 + \frac{a_1}{\varepsilon}(x_1 - \widehat{x}_1) \\ \dot{\widehat{x}}_2 = bu + \widehat{D} + \frac{a_2}{\varepsilon^2}(x_1 - \widehat{x}_1) \\ \dot{\widehat{D}} = \frac{a_3}{\varepsilon^3}(x_1 - \widehat{x}_1) \end{cases} \tag{9}$$

where $\widehat{\boldsymbol{x}} = [\widehat{x}_1 \ \ \widehat{x}_2 \ \ \widehat{D}]^{\mathrm{T}}$ represents the observer states and $\widehat{D}$ is the estimation of disturbance $D(t)$. In addition, the parameters ε, a_1, a_2, and a_3 are designed in the following analysis to ensure the state error is small as desired. The state error

$\boldsymbol{\rho} = [\rho_1\ \rho_2\ \rho_3]^{\mathrm{T}}$ is defined as the error between the actual state and the estimated state, i.e., $\rho_1 = (x_1 - \widehat{x}_1)/\varepsilon^2, \rho_2 = (x_2 - \widehat{x}_2)/\varepsilon, \rho_3 = D - \widehat{D}$.

Theorem 1: If the gain parameters a_1, a_2 and a_3 satisfy the following conditions: (i) $a_1, a_2, a_3 \in \mathbb{R}$ and $\varepsilon > 0$, $a_1, a_2, a_3 > 0$; (ii) $a_1 a_2 - a_3 > 0$. then, the state error $\boldsymbol{\rho}$ can converge to zero in the finite time using linear coordinate transformations.

Proof: For the designed observer [see (9)], the stability should be guaranteed. The estimation errors of observer are defined as

$$\boldsymbol{\rho} = [\rho_1\ \rho_2\ \rho_3]^{\mathrm{T}}. \tag{10}$$

Since

$$\begin{cases} \varepsilon\dot{\rho}_1 = \frac{\dot{x}_1 - \dot{\widehat{x}}_1}{\varepsilon} = -a_1\rho_1 + \rho_2 \\ \varepsilon\dot{\rho}_2 = \varepsilon\frac{\dot{x}_2 - \dot{\widehat{x}}_2}{\varepsilon} = -a_2\rho_1 + \rho_3 \\ \varepsilon\dot{\rho}_3 = \varepsilon(\dot{D} - \dot{\widehat{D}}) = -a_3\rho_1 + \varepsilon\dot{D} \end{cases} \tag{11}$$

then, the error system is rewritten as

$$\dot{\boldsymbol{\rho}} = \bar{A}\boldsymbol{\rho} + \bar{B}\dot{D} \tag{12}$$

where $\bar{A} = (1/\varepsilon)\begin{bmatrix} -a_1 & 1 & 0 \\ -a_2 & 0 & 1 \\ -a_3 & 0 & 0 \end{bmatrix}$, $\bar{B} = \begin{bmatrix} 0 \\ 0 \\ 1 \end{bmatrix}$.

The characteristic equation of $\bar{A}$ is

$$\left|\lambda I - \bar{A}\right| = \frac{1}{\varepsilon}\begin{vmatrix} \lambda + a_1 & -1 & 0 \\ a_2 & \lambda & -1 \\ a_3 & 0 & \lambda \end{vmatrix} = 0. \tag{13}$$

Then

$$\lambda^3 + a_1\lambda^2 + a_2\lambda + a_3 = 0.$$

If $a_i (i = 1, 2, 3)$ is chosen as below

$$\begin{cases} a_i (i = 1, 2, 3) > 0 \\ a_1 a_2 > a_3. \end{cases}$$

$\bar{A}$ is a Hurwitz matrix according to Hurwitz theory. Hence, the asymptotic stability of $\boldsymbol{\rho}$ can be guaranteed, which implies $\boldsymbol{\rho}$ can converge to zero in finite time using linear coordinate transformations [35]. ■

To alleviate peaking phenomenon caused by different initial values of the ESO, the small variable ε is designed as in [36]

$$\frac{1}{\varepsilon} = \begin{cases} 100t^3 & 0 \le t \le 1 \\ 100 & t > 1. \end{cases} \tag{14}$$

2) Convergent Speed Analysis: Based on (12), the solution can be obtained

$$\boldsymbol{\rho(t)} = e^{\bar{A}t}\boldsymbol{\rho(0)} + \int_0^t \bar{B}\dot{D}(\tau)e^{\bar{A}\tau}\mathrm{d}\tau. \tag{15}$$

Note that $D \le \|M\|$, therefore, we have

$$\begin{aligned} \|\boldsymbol{\rho(t)}\| &= \left\| e^{\bar{A}t}\boldsymbol{\rho(0)} + \int_0^t \bar{B}\dot{D}(\tau)e^{\bar{A}\tau}\mathrm{d}\tau \right\| \\ &\le \left\| e^{\bar{A}t}\boldsymbol{\rho(0)} \right\| + \left\| \int_0^t \bar{B}\dot{D}(\tau)e^{\bar{A}\tau}\mathrm{d}\tau \right\| \\ &\le \left\| e^{\bar{A}t}\boldsymbol{\rho(0)} \right\| + \|\bar{B}M\| \left\| \int_0^t e^{\bar{A}\tau}\mathrm{d}\tau \right\|. \end{aligned} \tag{16}$$

Since $\bar{A}$ is stable (Hurwitz matrix), so $\exists\Lambda, \varsigma > 0$ and $\Lambda, \varsigma \in \mathbb{R}$, s. t. $\|e^{\bar{A}t}\| \le \Lambda e^{-\varsigma t}$ and $\|\int_0^t e^{\bar{A}\tau}\mathrm{d}\tau\| \le \int_0^t \Lambda e^{-\varsigma t}\mathrm{d}\tau$, which implies if $t \to \infty$, then $\|e^{\bar{A}t}\boldsymbol{\rho(0)}\| \to 0$ and $\|\int_0^t e^{\bar{A}\tau}\mathrm{d}\tau\| \to 0$, respectively. Note that the convergence time is determined by $\bar{A}$. Thus we can adjust the gains parameters a_1, a_2 and a_3 to change the convergent speed, which can ensure the estimation accuracy of the observer.

B. Double Loop Integral Sliding Mode Controller Design

1) Inner-Loop Sliding Mode Controller Design: The inner-loop is designed as the ET opening angle change loop shown in Fig. 2. Suppose ω_d is the desired value of the inner-loop, and the error of the inner-loop is defined as

$$\omega_e = \omega_d - x_2. \tag{17}$$

Let the sliding mode surface be defined as in [37]–[41]

$$s_{in} = \omega_e + k_1\int_0^t \omega_e\mathrm{d}t \tag{18}$$

where $k_1 \in \mathbb{R}$ and $k_1 > 0$. Then

$$\begin{aligned} \dot{s}_{in} =& \dot{\omega}_e + k_1\omega_e = \dot{\omega}_d - \dot{x}_2 + k_1\omega_e \\ =& \dot{\omega}_d - a_{21}(x_1 - \theta_0) - a_{22}x_2 - bu + k_1\omega_e \\ & - \kappa_1\mathbf{sgn}(x_1 - \theta_0) - \kappa_2\mathbf{sgn}(x_2) - D. \end{aligned} \tag{19}$$

When the sliding mode of the system approaches the switching surface, then $s_{in} = 0$. And, according to (18), we obtain

$$\omega_e + k_1\int_0^t \omega_e\mathrm{d}t = 0.$$

Then

$$\omega_e = \eta\exp(-k_1 t) \tag{20}$$

where η is a constant determined by initial condition. Since $k_1 > 0$, if $t \to \infty$, then $\omega_e \to 0$, where the convergence time is determined by k_1. Consequently, we also obtain $k_1\int_0^t \omega_e\mathrm{d}t \to 0$.

Therefore, the candidate Lyapunov function of inner-loop controller can be chosen as in [39]–[41]

$$V_1 = \frac{1}{2}s_{in}^2. \tag{21}$$

Then

$$\begin{aligned}\dot{V}_1 &= s_{in}\dot{s}_{in}\\ &= s_{in}(\dot{\omega}_d - a_{21}(x_1-\theta_0) - a_{22}x_2 - \kappa_2\mathbf{sgn}(x_2)\\ &\quad - bu - \kappa_1\mathbf{sgn}(x_1-\theta_0) - D + k_1\omega_e).\end{aligned} \tag{22}$$

In terms of (22), the inner-loop control law can be designed as

$$\begin{aligned}u = \frac{1}{b}\Big(&\dot{\omega}_d - a_{21}(x_1-\theta_0) - a_{22}x_2 - \kappa_1\mathbf{sgn}(x_1-\theta_0)\\ &- \kappa_2\mathbf{sgn}(x_2) - \widehat{D} + k_1\omega_e + \lambda_1 s_{in} + \beta_1\mathbf{sgn}(s_{in})\Big)\end{aligned} \tag{23}$$

where λ_1 and β_1 are positive constants, so

$$\begin{aligned}\dot{V}_1 &= s_{in}\dot{s}_{in}\\ &= s_{in}\left(\widehat{D} - D - \lambda_1 s_{in} - \beta_1\mathbf{sgn}(s_{in})\right).\end{aligned} \tag{24}$$

Hence

$$\dot{V}_1 = \left(\widehat{D} - D\right)s_{in} - \lambda_1 s_{in}^2 - \beta_1\left|s_{in}\right|.$$

If $\dot{V}_1 \le 0$, we obtain $\beta_1 \ge (\widehat{D} - D)$.

By replacing the unmeasurable variable x_2 with its estimated value $\widehat{x}_2$, we obtain the following inner-loop controller based on the observer:

$$\begin{aligned}u = \frac{1}{b}\Big(&\dot{\omega}_d - a_{21}(x_1-\theta_0) - a_{22}\widehat{x}_2 - \kappa_1\mathbf{sgn}(x_1-\theta_0)\\ &- \kappa_2\mathbf{sgn}(\widehat{x}_2) - \widehat{D} + k_1\omega_e + \lambda_1 s_{in} + \beta_1\mathbf{sgn}(s_{in})\Big).\end{aligned} \tag{25}$$

2) Outer-Loop Sliding Mode Controller Design: The outer-loop is designed as the ET opening angle loop shown in Fig. 2 and x_d is the desired value of outer-loop. The error of outer-loop is defined as

$$\theta_e = x_d - x_1. \tag{26}$$

The sliding mode surface is defined as [37]–[41]

$$s_{ou} = \theta_e + k_2\int_0^t \theta_e \mathrm{d}t \tag{27}$$

where $k_2 \in \mathbb{R}$ and $k_2 > 0$. Then

$$\dot{s}_{ou} = \dot{\theta}_e + k_2\theta_e = \dot{x}_d - \dot{x}_1 + k_2\theta_e. \tag{28}$$

According to the analysis of inner-loop control law, we obtain $\dot{x}_1 = \omega_d + \xi$ when $\omega_e \to 0$ and $\xi \in \mathbb{R}$ and $\xi > 0$. Then

$$\dot{s}_{ou} = \dot{\theta}_e + k_2\theta_e = \dot{x}_d - \omega_d - \xi + k_2\theta_e. \tag{29}$$

Based on (29), the outer-loop control law is designed as

$$\omega_d = \dot{x}_d + k_2\theta_e + \beta_2\mathbf{sgn}(s_{ou}) \tag{30}$$

where β_2 is a positive constant.

Substituting (30) into (29), we have

$$\dot{s}_{ou} = -\beta_2\mathbf{sgn}(s_{ou}) - \xi.$$

Then

$$s_{ou}\dot{s}_{ou} = -\beta_2\left|s_{ou}\right| - \xi s_{ou}. \tag{31}$$

TABLE I
ET PARAMETERS VALUES

Parameters	Value	Units
θ_0	2	degree
k_l	16.95	—
k_t	0.016	N · m/A
k_{pre}	0.107	N · m
R_a	2.8	Ω
J	1.15×10^{-3}	kg · m^2
k_{tf}	0.0048	N · m
k_{ch}	2.4	—
k_v	0.016	V · s/rad
k_f	4×10^{-4}	V · m · s/rad
k_{sp}	0.0247	V · m/rad

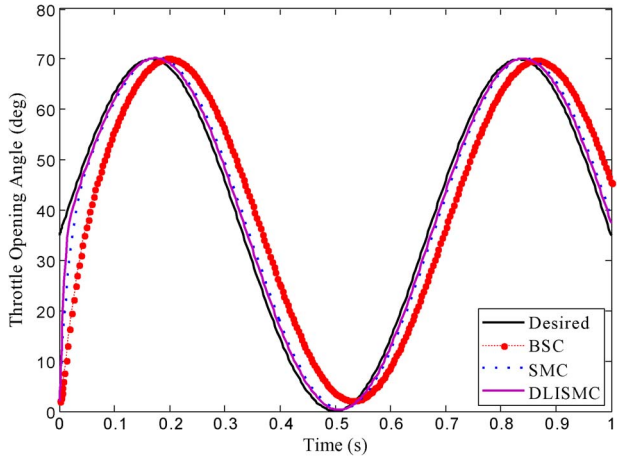

Fig. 4. Tracking response of the sinusoidal signal.

If the gain is high enough and $\beta_2 \ge \|\xi\|$, then $s_{ou}\dot{s}_{ou} < 0$. Therefore, the sliding mode tends to converge toward the surface $s_{ou} = 0$ in finite time [42], [43].

To alleviate the undesirable chattering noise caused by $\mathbf{sgn}(s)$, a saturation function $\mathbf{sat}(s)$ is used to replace sign function, which is expressed as [42], [44], [45]

$$\mathbf{sat}(s) = \begin{cases} 1, & s > \Delta \\ s/\Delta, & |s| < \Delta \\ -1, & s < \Delta. \end{cases} \tag{32}$$

IV. NUMERICAL EXPERIMENTS

Simulation-based numerical experiments are carried out using parameters according to [22] as shown in Table I. To analyze the performance, in terms of accuracy and responsiveness, of the designed DLISMC controller for the ET valve, it is compared with the SMC in [21], and the back-stepping control (BSC) in [22]. For the ESO, the parameters of the observer are chosen as follows: $a_1 = 6, a_2 = 11$, and $a_3 = 6$. In addition, the parameters of the inner-loop and outer-loop controllers are given as: $k_1 = 1$, $\beta_1 = 1.5$, $\lambda_1 = 1200$, $k_2 = 0.3$, and $\beta_2 = 15$.

A. Observer Performance Verification

In this section, the tracking performance of a sinusoidal reference signal is analyzed as shown in Figs. 4 and 5. From the

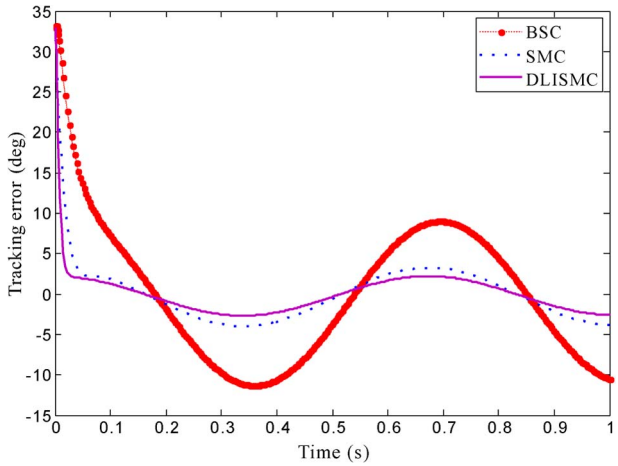

Fig. 5. Tracking error of the sinusoidal signal.

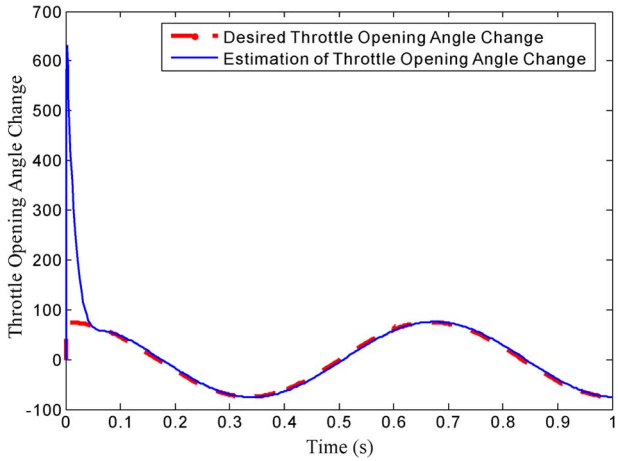

Fig. 6. Estimation of throttle opening angle change.

viewpoint of response time, the performance of the proposed controller is better than those of the other two as shown in Fig. 4. From the accuracy viewpoint, as shown in Fig. 5, the tracking errors of the SMC and BSC reach the negative and positive maximums at 0.35 s and 0.68 s, respectively. By contrast, the tracking error distribution of the proposed DLISMC is relatively steady and its tracking errors are smaller than those of the SMC and BSC.

Figs. 6 and 7 illustrate the estimation of the ET angular velocity and disturbance, respectively. Fig. 6 shows that the ESO can estimate the ET angular velocity precisely. Fig. 7 illustrates the ability of the observer to compensate the influence of the torque produced by the gear of ET and the influence of external disturbance.

B. Analysis of Controller Robustness

Fig. 8 shows the step-tracking performance for the three controllers. The settling time is analyzed due to the requirement of no overshoot, where the settling time is defined as the time taken by a signal to reach and stay within a range of 2% of the step height. The settling times of the SMC, BSC and DLISMC are about 0.0985 s, 0.1812 s, and 0.0894 s, respectively. Hence, the tracking response time of the DLISMC is smaller than those of the SMC and BSC. Therefore, the proposed controller

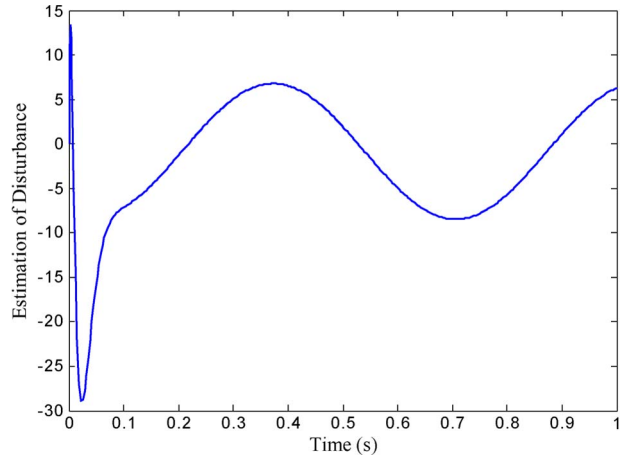

Fig. 7. Estimation of disturbance.

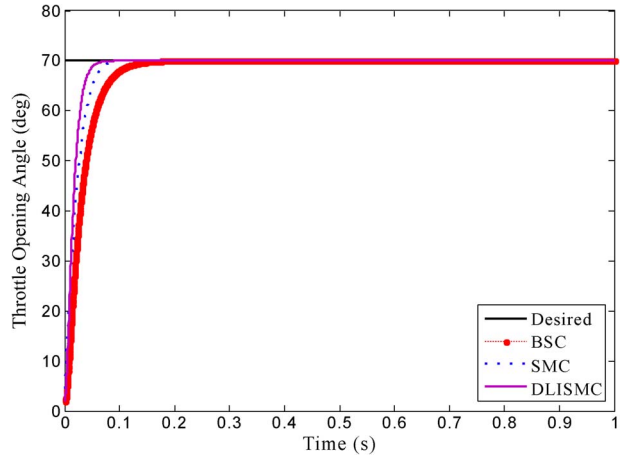

Fig. 8. Tracking response of step signal.

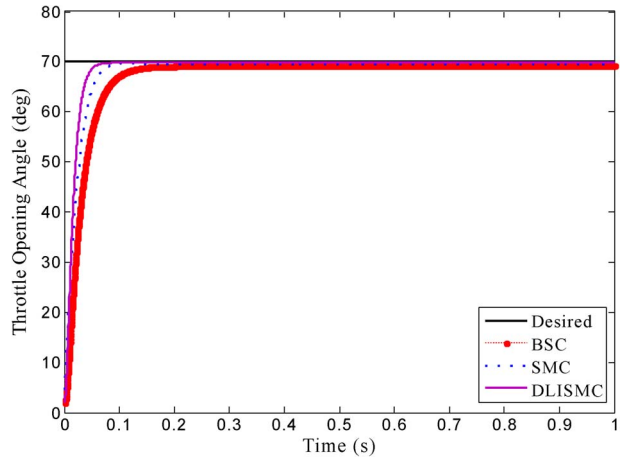

Fig. 9. Step signal tracking response of parameters change.

can more quickly reach the desired value and become stable compared with those under SMC and BSC, which indicates that the ET can respond quickly in the case of parametric variation.

To analyze the robustness performance of these controllers, simulations with parametric variations are considered here: k_t is varied from 0.016 to 0.0128, k_{tf} from 0.0048 to 0.02964, and k_{sp} from 0.0247 to 0.0576 according to [22]. Figs. 9 and 10 show the step-tracking performance of the three controllers

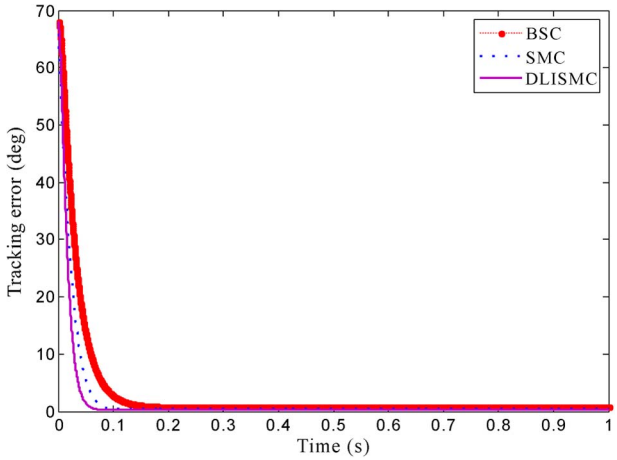

Fig. 10. Step signal tracking error of parameters change.

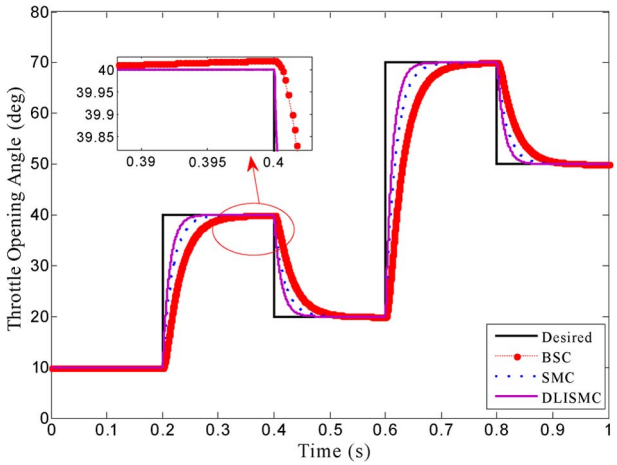

Fig. 11. Setpoint signal tracking response.

with these parametric variations. The tracking errors of the SMC, BSC, and DLISMC are about 0.5 deg, 0.9 deg, and 0.2 deg, respectively. It indicates that the accuracy of the proposed controller is higher than those of the SMC and BSC. In addition, from Figs. 8 and 9, it can be observed that the performance of SMC and BSC becomes worse under parametric variations, whereas the DLISMC is robust to parametric variations.

The discussion heretofore suggests that the proposed controller has strong robustness relative to parametric uncertainties and can also satisfy engineering practice requirements [10]. Further, a stable vehicle speed can be guaranteed as the adaptive controller can adjust the opening angle of the ET valve in a timely manner when an external disturbance occurs, which can aid a vehicle platoon under V2V communications to respond accordingly and improve its robustness.

C. Controller Performance for Setpoint

In practice, sudden changes of the signal are possible from small to large opening angles or vice versa, which are important to engine control. Moreover, there exists the phenomenon of stop-and-go in traffic flow when congestion occurs. Vehicle speed can change rapidly or slowly under stop-and-go traffic flows, which implies that the ET valve should be capable of responding in a timely manner. However, the nonlinear spring

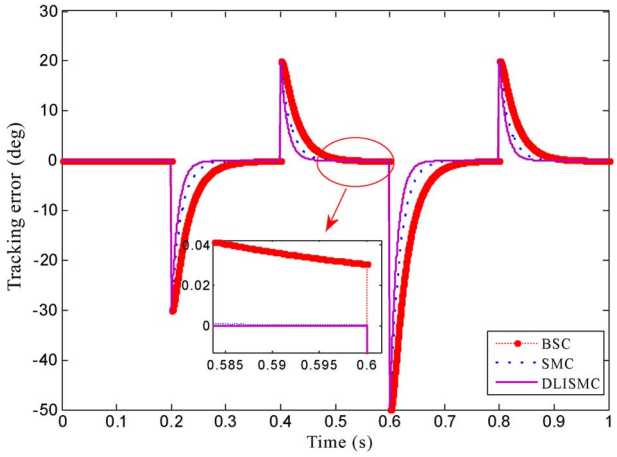

Fig. 12. Setpoint signal tracking error.

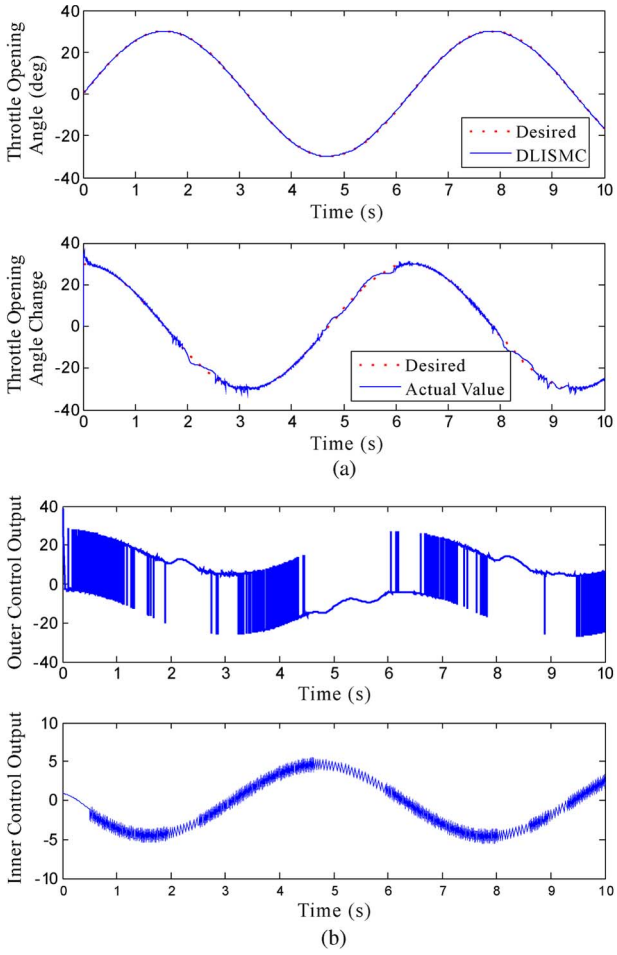

Fig. 13. Performance with sign function: (a) opening angle and opening angle change, (b) outer and inner control output.

does not allow opening angles below 5° and above 80° [21]. Hence, the minimum and maximum values of the setpoint signal are chosen as 10° and 70°, respectively.

Figs. 11 and 12 show the setpoint signal tracking performance for these three controllers using the rising and falling times. The rising time is defined as the time taken by a signal to change from 10% to 90% of the step height. In Fig. 11, the rising times of the SMC, BSC, and DLISMC are about 0.0398 s, 0.0597 s, and 0.0276 s, respectively. Hence, the rising time with

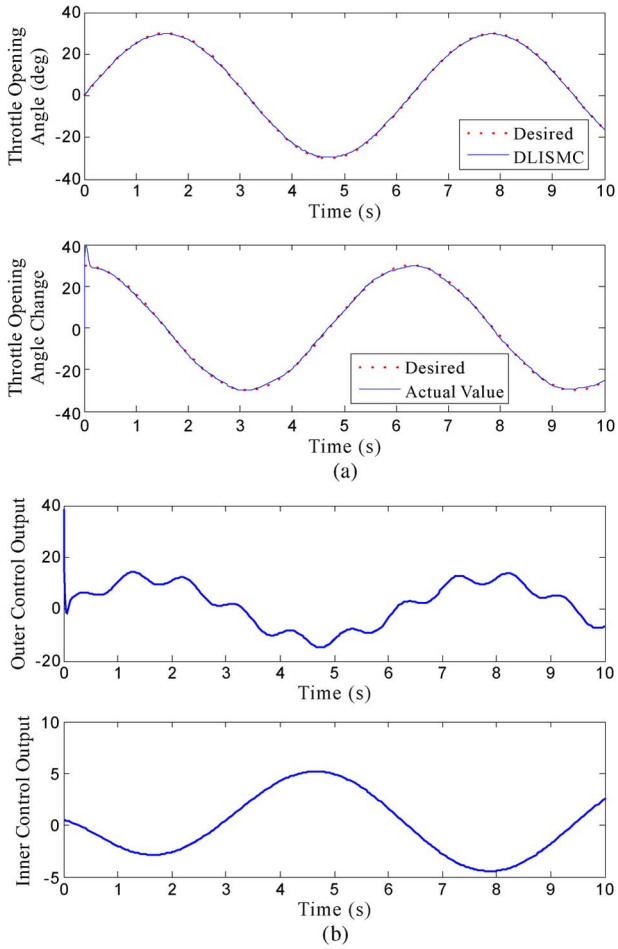

Fig. 14. Performance with saturation function: (a) opening angle and opening angle change, (b) outer and inner control output, ($\Delta = 0.5$).

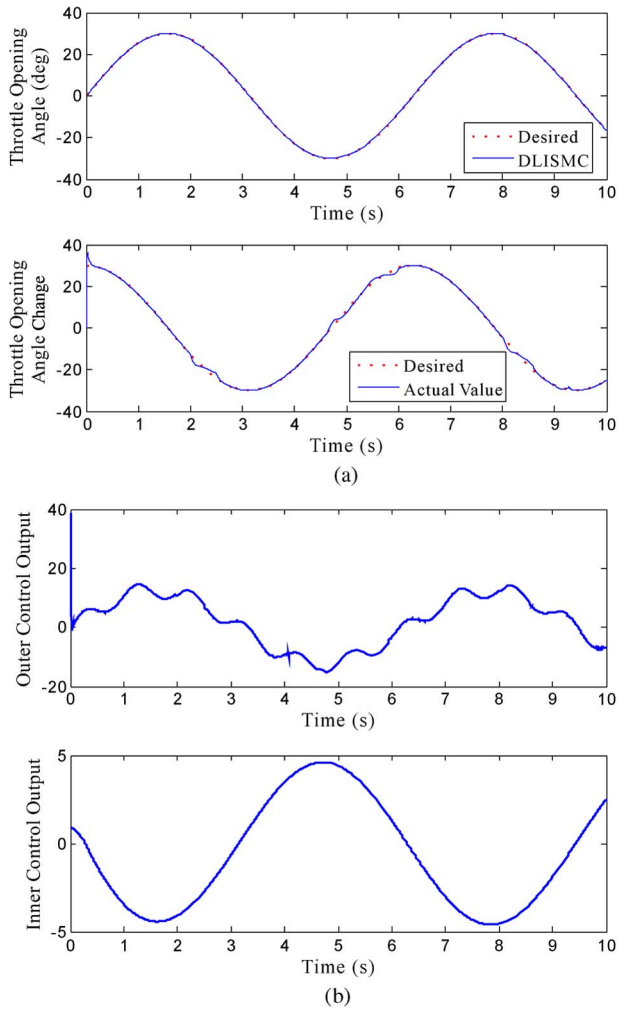

Fig. 15. Performance with saturation function: (a) opening angle and opening angle change, (b) outer and inner control output, ($\Delta = 0.05$).

the DLISMC is smaller than those under SMC and BSC. The falling time is defined as the time taken by a signal to change from 90% to 10% of the step height [21]. The falling times of SMC, BSC, and DLISMC in Fig. 12 are about 0.0400 s, 0.0603 s, and 0.0274 s, respectively. Hence, the falling time with the DLISMC is also smaller than those under SMC and BSC. In summary, the performance of the proposed controller is better than that of the SMC and BSC with respect to accuracy and responsiveness under sudden non-smooth signal variation.

D. Saturation Function's Influence on Controller

To address the chattering problem, the sign function is replaced by a saturation function, and numerical experiments are conducted to analyze the effects of the sign and saturation functions on the controller, as shown in Figs. 13 and 14 under the sinusoidal reference input within 10s. Figs. 13(a) and 14(a) show the chattering under the throttle opening angle change with the sign function. The sign function and the saturation function have little effect on the throttle opening angle tracking. Moreover, Figs. 13(b) and 14(b) illustrate that the chattering phenomenon is reduced when the sign function is replaced by the saturation function.

Figs. 14 and 15 show the control performance under the saturation function with $\Delta = 0.5$ and $\Delta = 0.05$, respectively. From Figs. 14 and 15, the variation of Δ has little effect on the throttle opening angle tracking and control input. However, when Δ decreases, the tracking performance of the throttle opening angle change deteriorates and a little chattering occurs in the inner-loop and outer-loop control law.

E. Controller Performance Comparison

Table II summarizes the performance of the three controllers under different input signals. It illustrates that all three controllers can track step signal without overshoot. However, with respect to the settling time, the proposed controller can reach the desired value and become stable more quickly than SMC and BSC, which implies that the vehicle speed can quickly become stable as the vehicle speed is associated with the throttle opening angle [4]. Furthermore, when the ET parameters (k_t, k_{tf}, and k_{sp}) change, the tracking errors of DLISMC, SMC and BSC are 0.2 deg, 0.5 deg, and 0.9 deg, respectively. This indicates that the proposed controller has better robustness than SMC and BSC, which can guarantee the practical string stability of vehicle platoon under V2V communications and also satisfy the robustness requirement in engineering practice.

The rising times of SMC, BSC, and DLISMC are 0.0398 s, 0.0597 s, and 0.0276 s, respectively, with the setpoint signal.

TABLE II
CONTROLLER PERFORMANCE COMPARISON

Inputs / Controllers	Sine signal	Step signal			Setpoint signal	
	Tracking errors (deg)	Overshoot	No changes in parameter values	Changes in parameter values	Rising time (s)	Falling time(s)
			Settling time (s)	Tracking errors (deg)		
SMC in Ref. [21]	$[-3.95, 3.26]$	no	0.0985	0.5	0.0398	0.0400
BSC in Ref. [22]	$[-11.26, 9.04]$	no	0.1812	0.9	0.0597	0.0603
DLISMC	$[-2.66, 2.22]$	no	0.0894	0.2	0.0276	0.0274

Hence, the proposed controller can reach the desired value in the shortest time when the signal amplitude increases suddenly. While the falling times of SMC, BSC, and DLISMC are 0.0400 s, 0.0603 s, and 0.0274 s, respectively. Hence, these two controllers cannot track the desired signal accurately when signal amplitude is changed from high to low.

Based on above discussion, we conclude that the accuracy and responsiveness of the proposed controller are better than those of the BSC and SMC with respect to tracking errors and rising/falling time or settling time under the sinusoidal, step or setpoint signals.

V. CONCLUSION

To enhance the accuracy and responsiveness of ETC, an ESO based double loop integral sliding mode controller is proposed in this paper. First, the ESO is used to estimate the throttle opening angle change and disturbance. Then, a DLISMC controller is proposed, including the inner loop based on throttle opening angle change errors and outer loop based on throttle opening angle errors. Finally, numerical experiments are conducted with three different reference signals for the DLISMC, and compared with those for the BSC and SMC. The results illustrate that the ESO has performed well in terms of estimating the throttle opening angle change and disturbance. Further, compared with the SMC and BSC, the accuracy and responsiveness of the proposed DLISMC controller are improved with respect to tracking errors and rising/falling time or settling time under three different reference signals. Hence, the proposed DLISMC controller can perform relatively better under the V2V communications context related to platoon stability.

REFERENCES

[1] V. Milanés *et al.*, "Cooperative adaptive cruise control in real traffic situations," *IEEE Trans. Intell. Transp. Syst.*, vol. 15, no. 1, pp. 296–305. Feb. 2014.

[2] S. Ukkusuri, Y. Wang, and T. Chigan, "Guest editorial for special issue on exploiting wireless communication technologies in vehicular transportation networks," *IEEE Trans. Intell. Transp. Syst.*, vol. 12, no. 3, pp. 633–634, Sep. 2011.

[3] D. Sun, Y. Li, W. Liu, M. Zhao, and X. Liao, "Research summary on transportation cyber physical systems and the challenging technologies," *Chin. J. Highway Transp.*, vol. 26, no. 1, pp. 0144–0155, Jan. 2013.

[4] P. Ioannou and Z. Xu, "Throttle and brake control system for automatic vehicle following," *Intell. Veh. Highway Syst. J.*, vol. 1, no. 4, pp. 345–377, Apr. 1994.

[5] K. Li and P. Ioannou, "Modeling of traffic flow of automated vehicles," *IEEE Trans. Intell. Transp. Syst.*, vol. 5, no. 2, pp. 99–113, Jun. 2004.

[6] J. K. Hedrick, D. McMahon, V. Narendran, and D. Swaoop, "Longitudinal vehicle controller design for IVHS system," in *Proc. Amer. Control Conf.*, Jun. 1991, vol. 3, pp. 3107–3112.

[7] X. H. Jiao, J. Y. Zhang, and T. L. Shen, "An adaptive servo control strategy for automotive electronic throttle and experimental validation," *IEEE Trans. Ind. Electron.*, vol. 61, no. 11, pp. 6275–6284, Nov. 2014.

[8] X. F. Yuan and Y. N. Wang, "A novel electronic-throttle-valve controller based on approximate model method," *IEEE Trans. Ind. Electron.*, vol. 56, no. 3, pp. 883–890, Mar. 2009.

[9] D. Kim, H. Peng, S. Bai, and J. M. Maguire, "Control of integrated powertrain with electronic throttle and automatic transmission," *IEEE Trans. Contr. Syst. Technol.*, vol. 15, no. 3, pp. 474–482, May 2007.

[10] J. Deur, D. Pavković, N. Perić, M. Jansz, and D. Hrovat, "An electronic throttle control strategy including compensation of friction and limp-home effects," *IEEE Trans. Ind. Appl.*, vol. 40, no. 3, pp. 821–834, May/Jun. 2004.

[11] J. Ploeg, N. V. D. Wouw, and H. Nijmeijer, "L_p string stability of cascaded systems: Application to vehicle platooning," *IEEE Trans. Contr. Syst. Technol.*, vol. 22, no. 2, pp. 786–793, Mar. 2014.

[12] W. Wang, S. S. Liao, X. Li, and J. S. Ren, "The process of information propagation along a traffic stream through intervehicle communication," *IEEE Trans. Intell. Transp. Syst.*, vol. 15, no. 1, pp. 345–354, Feb. 2014.

[13] L. Xiao, and F. Gao, "Practical string stability of platoon of adaptive cruise control vehicles," *IEEE Trans. Intell. Transp. Syst.*, vol. 12, no. 4, pp. 1184–1194, Dec. 2011.

[14] X. Yuan and Y. Wang, "Neural networks based self-learning PID control of electronic throttle," *Nonlinear Dyn.*, vol. 55, no. 4, pp. 385–393, Mar. 2009.

[15] Y. H. Zweiri, J. F. Whidborne, K. Althoefer, and L. D. Seneviratne, "A new three-term backpropagation algorithm with convergence analysis," in *Proc. IEEE Int. Conf. Robot. & Autom.*, Washington, DC, USA, May 2002, pp. 3882–3887.

[16] M. S. Al-Batah, N. A. M. Isa, K. Z. Zamli, and A. Azizli, "Modified recursive least squares algorithm to train the hybrid multilayered perceptron (HMLP) network," *Appl. Soft Comput.*, vol. 10, no. 1, pp. 236–244, Jan. 2010.

[17] S. A. Billings and H. B. Jamaluddin, "A comparison of the backpropagation and recursive prediction error algorithms for training neural networks," *Mech. Syst. Signal Process.*, vol. 5, no. 3, pp. 233–255, May 1991.

[18] W. Sheng and Y. Bao, "Fruit fly optimization algorithm based fractional order fuzzy-PID controller for electronic throttle," *Nonlinear Dyn.*, vol. 73, no. 1–2, pp. 611–619, Jul. 2013.

[19] A. K. Yadav, and P. Gaur, "Robust adaptive speed control of uncertain hybrid electric vehicle using electronic throttle control with varying road grade," *Nonlinear Dyn.*, vol. 76, no. 1, pp. 305–321, Apr. 2014.

[20] M. Barić, I. Petrović, and N. Perić, "Neural network-based sliding mode control of electronic throttle," *Eng. Appl. Artif. Intell.*, vol. 18, no. 8, pp. 951–961, Dec. 2005.

[21] Y. D. Pan, Ü. Özgüner, and O. H. Dağci, "Variable-structure control of electronic throttle valves," *IEEE Trans. Ind. Electron.*, vol. 55, no. 11, pp. 3899–3907, Nov. 2008.

[22] H. Chen, Y. F. Hu, H. Z. Guo, and H. T. Song, "Control of electronic throttle based on backstepping approach," *Control Theory & Appl.*, vol. 28, no. 4, pp. 491–496, Apr. 2011.

[23] M. Vašak, M. Baotić, M. Morari, I. Petrović, and N. Perić, "Constrained optimal control of an electronic throttle," *Int. J. Control*, vol. 79, no. 5, pp. 465–478, May/Jun. 2006.

[24] M. Vašak, M. Baotić, I. Petrović, and N. Perić, "Hybrid theory-based time-optimal control of an electronic throttle," *IEEE Trans. Ind. Electron.*, vol. 54, no. 3, pp. 1483–1494, Jun. 2007.

[25] X. F. Yuan, Y. N. Wang, W. Sun, and L. H. Wu, "RBF networks-based adaptive inverse model control system for electronic throttle," *IEEE Trans. Control Syst. Technol.*, vol. 18, no. 3, pp. 750–756, May 2010.

[26] X. Yuan, Y. Wang, L. Wu, X. Zhang, and W. Sun, "Neural network based self-Learning control strategy for electronic throttle valve," *IEEE Trans. Veh. Technol.*, vol. 59, no. 8, pp. 3757–3765, Oct. 2010.

[27] C. Wang, and D. Huang, "A new intelligent fuzzy controller for nonlinear hysteretic electronic throttle in modern intelligent automobiles," *IEEE Trans. Ind. Electron.*, vol. 60, no. 6, pp. 2332–2345, Jun. 2013.

[28] P. Mercorelli, "A hysteresis hybrid extended kalman filter as an observer for sensorless valve control in camless internal combustion engines," *IEEE Trans. Ind. Appl.*, vol. 48, no. 6, pp. 1940–1949, Nov./Dec. 2012.
[29] J. V. Gorp, M. Defoort, K. C. Veluvolu, and M. Djemai, "Hybrid sliding mode observer for switched linear systems with unknown input," *J. Franklin Instit.*, vol. 351, no. 7, pp. 3987–4008, Jul. 2014.
[30] P. Mercorelli, "A two-stage augmented extended kalman filter as an observer for sensorless valve control in camless internal combustion engines," *IEEE Trans. Ind. Electron.*, vol. 59, no. 11, pp. 4236–4247, Nov. 2012.
[31] Y. Zhao, W. Qiao, and L. Wu, "An adaptive quasi-sliding-mode rotor position observer-based sensorless control for interior permanent magnet synchronous machines," *IEEE Trans. Power Electron.*, vol. 28, no. 12, pp. 5618–5629, Dec. 2013.
[32] J. Yao, Z. Jiao, and D. Ma, "Adaptive robust control of DC motors with extended state observer," *IEEE Trans. Ind. Electron.*, vol. 61, no. 7, pp. 3630–3637, Jul. 2014.
[33] B. Guo and Z. Zhao, "On convergence of nonlinear extended state observer for multi-input multi-output systems with uncertainty," *IET Control Theory & Appl.*, vol. 6, no. 15, pp. 2375–2386, Oct. 2012.
[34] S. Li, J. Yang, W. Chen, and X. Chen, "Generalized extended state observer based control for systems with mismatched uncertainties," *IEEE Trans. Ind. Electron.*, vol. 59, no. 12, pp. 4792–4802, Dec. 2012.
[35] Z. J. Kang and X. Y. Chen, "A design method of nonlinear extension state observer," *Electr. Mach. Control*, vol. 5, no. 3, pp. 199–203, Sep. 2001.
[36] J. N. Teoh, C. Du, G. Guo, and L. Xie, "Rejecting high frequency disturbances with disturbance observer and phase stabilized control," *Mechatronics*, vol. 18, no. 1, pp. 53–60, Feb. 2008.
[37] F. Castaños, D. Hernández, and L. M. Fridman, "Integral sliding-mode control for linear time-invariant implicit systems," *Automatica*, vol. 50, no. 3, pp. 971–975, Mar. 2014.
[38] L. Wu, X. Su, and P. Shi, "Sliding mode control with bounded L_2 gain performance of Markovian jump singular time-delay systems," *Automatica*, vol. 48, no. 8, pp. 1929–1933, Aug. 2012.
[39] P. Mercorelli, "An antisaturating adaptive pre-action and a slide surface to achieve soft landing control for electromagnetic actuators," *IEEE/ASME Trans. Mechatron.*, vol. 17, no. 1, pp. 76–85, Feb. 2012.
[40] J. D. Lee and R. Y. Duan, "Cascade modeling and intelligent control design for an electromagnetic guiding system," *IEEE/ASME Trans. Mechatron.*, vol. 16, no. 3, pp. 470–479, Jun. 2011.
[41] A. Pisano, A. Davila, L. Fridman, and E. Usai, "Cascade control of PM DC drives via second-order sliding-mode technique," *IEEE Trans. Ind. Electron.*, vol. 55, no. 11, pp. 3846–3854, Nov. 2008.
[42] G. L. Wang, R. F. Yang, and D. G. Xu, "DSP-based control of sensorless IPMSM drives for wide-speed-range operation," *IEEE Trans. Ind. Electron.*, vol. 60, no. 2, pp. 720–727, Feb. 2013.
[43] Z. Xu and M. F. Rahman, "Comparison of a sliding observer and a kalman filter for direct-torque-controlled IPM synchronous motor drives," *IEEE Trans. Ind. Electron.*, vol. 59, no. 11, pp. 4179–4188, Nov. 2012.
[44] Z. W. Qiao *et al.*, "New sliding-mode observer for position sensorless control of permanent-magnet synchronous motor," *IEEE Trans. Ind. Electron.*, vol. 60, no. 2, pp. 710–719, Feb. 2013.
[45] F. Lin, S. Chen, and M. Huang, "Intelligent double integral sliding-mode control for five-degree-of-freedom active magnetic bearing system," *IET Control Theory & Appl.*, vol. 5, no. 11, pp. 1287–1303, Jul. 2011.

Yongfu Li received the B.S. degree in measuring and control technology and instrumentations from Xian University of Science and Technology, Xian, China, in 2007 and the Ph.D. degree in control theory and control engineering from Chongqing University, Chongqing, China, in 2012.

Since April 2014, he has been a Postdoctoral Researcher with NEXTRANS Center, Purdue University, West Lafayette, IN, USA. He is currently an Associate Professor of control science and engineering with Chongqing University of Posts and Telecommunications, Chongqing, China. His research interests include intelligent transportation systems, automotive electronics, and control theory. Dr. Li has served as a Reviewer for more than 20 international journals or conferences such as IEEE TRANSACTIONS ON INTELLIGENT TRANSPORTATION SYSTEMS, *Nonlinear Dynamics*, *Journal of Advanced Transportation*, *International Journal of Dynamics and Control*, *International Journal of Communication Systems*, International Federation of Automatic Control World Congress, CCC, and so on.

Bin Yang received the B.S. degree in mechanical design and manufacturing automation from Chongqing University of Posts and Telecommunications, Chongqing, China, in 2012. He is currently working toward the M.S. degree in mechanical and electrical engineering at Chongqing University of Posts and Telecommunications.

His research interests include engine control and intelligent transportation systems.

Taixiong Zheng received the B.S. and M.S. degrees in material processing engineering and the Ph.D. degree in mechanical engineering from Chongqing University, Chongqing, China, in 1997, 2000, and 2003, respectively.

He is currently a Professor of control science and engineering with Chongqing University of Posts and Telecommunications, Chongqing, China. His research interests include engine control and vehicle active safe control.

Yinguo Li received the Ph.D. degree in automatic control from Chongqing University, Chongqing, China, in 1996.

He is currently a Professor and the President with Chongqing University of Posts and Telecommunications, Chongqing, China. He is also the Director of the Center for Automotive Electronics and Embedded System Engineering. His research interests include automotive electronics, intelligent transportation systems (ITS), and engine control.

Mingyue Cui received the B.S. degree in automation engineering from Luoyang University of Science and Technology, Luoyang, China, in 1998; the M.S. degree in control theory and control engineering from Lanzhou University of Technology, Lanzhou, China, in 2009; and the Ph.D. degree in control theory and control engineering from Chonqging University, Chonqging, in 1998, 2009, and 2012, respectively.

He is currently a Lecturer of control science and engineering with Nanyang Normal University, Nanyang, China. His research interests include mobile robot control and vibration active control.

Srinivas Peeta received the B.S. degree from the Indian Institute of Technology, Madras, India, in 1988; the M.S. degree from California Institute of Technology, Pasadena, CA, USA, in 1989; and the Ph.D. degree from the University of Texas at Austin, Austin, TX, USA, in 1994, all in civil engineering.

He is currently a Professor of civil engineering with Purdue University, West Lafayette, IN, USA, and the Director of NEXTRANS Center, the U.S. Department of Transportation Region 5 University Transportation Center, USA. His research interests include intelligent transportation systems, operations research, control theory, and computational intelligence techniques. Dr. Peeta serves on the editorial advisory boards of the journals *Transportation Research Part B*, *Intelligent Transportation Systems Journal*, and *Transportmetrica B*. He serves as the Area Editor for transport telematics for *Networks and Spatial Economics*. He previously served as the Chair of the Transportation Network Modeling Committee of the Transportation Research Board of the National Academies. He is also a member of International Federation of Automatic Control Technical Committee on Transportation Systems.